Applied Radiation and Isotopes 190 (2022) 110508

Contents lists available at ScienceDirect

Applied Radiation and Isotopes

journal homepage: www.elsevier.com/locate/apradiso

Towards *in vivo* applications of ^{111}Ag perturbed angular correlation of γ-rays (PAC) spectroscopy

Marianna Tosato [a], Mattia Asti [b], Valerio Di Marco [a], Marianne L. Jensen [c], Juliana Schell [d,e], Thien Thanh Dang [e], Ulli Köster [f], Mikael Jensen [g], Lars Hemmingsen [h,*]

[a] Department of Chemical Sciences, University of Padova, via Marzolo 1, 35131, Padova, Italy
[b] Radiopharmaceutical Chemistry Section, Nuclear Medicine Unit, AUSL-IRCCS di Reggio Emilia, via Amendola 2, 42122, Reggio Emilia, Italy
[c] The Niels Bohr Institute, University of Copenhagen, Universitetsparken 5, 2100, København Ø, Denmark
[d] European Organization for Nuclear Research (CERN), 1211, Geneva, Switzerland
[e] Institute for Materials Science and Center for Nanointegration Duisburg-Essen (CENIDE), University of Duisburg-Essen, 45141, Essen, Germany
[f] Institut Laue-Langevin, 71 avenue des Martyrs, 38042, Grenoble, France
[g] The Hevesy Laboratory, Dept. Health Technology, Technical University of Denmark (DTU), Frederiksborgvej 399, 4000, Roskilde, Denmark
[h] Department of Chemistry, University of Copenhagen, Universitetsparken 5, 2100, København Ø, Denmark

A B S T R A C T

^{111}Ag-perturbed angular correlation of γ-rays (PAC) spectroscopy provides information on the nuclear quadrupole interactions, and thereby on the local structure and dynamics of the silver ion binding site. Brownian rotational motion, *i.e.* rotational diffusion, of ^{111}Ag-labeled molecules will significantly affect the PAC spectra. Here we illustrate this effect, by simulating ^{111}Ag PAC spectra for ^{111}Ag-labeled molecules with molecular masses spanning from 10^2 to 10^6 g/mol, reflecting a span from fast (small molecules) to slow (large molecules) rotational diffusion on the PAC time scale. The simulated spectra are compared to ^{111}Ag-PAC data obtained from a pilot study involving ^{111}Ag(I) bound to a designed chelator exhibiting fast reorientation in solution, as well as to ^{111}Ag-labeled species formed by ^{111}Ag(I) in human serum, exhibiting slow (or no) reorientation on the PAC time scale. The simulated and experimental data illustrate typical PAC signals that are likely to be observed *in vivo,* when following the fate of ^{111}Ag-labeled compounds. Potential *in vivo* applications are stability studies of ^{111}Ag-radiopharmaceuticals, dissociation studies of ^{111}Ag from the labeled molecule followed by binding to another (bio)molecule, or binding of ^{111}Ag-labeled probes to larger carriers such as proteins.

1. Introduction

Perturbed Angular Correlation (PAC) spectroscopy has been applied within nuclear- and solid-state physics as well as biochemistry for decades (Frauenfelder and Steffen, 1965; Hemmingsen et al., 2004) including a number of publications within radiopharmacy and *in vivo* studies (Derksen et al., 1988; Forssen, 1997; Hwang and Mauk, 1977; Kurakina et al., 2020; Maurk and Gamble, 1979; 1980; Meares and Westmoreland, 1971; Roerdink et al., 1989).

In PAC spectroscopy the correlation, in time and space, between two γ-rays emitted in succession from a radionuclide is measured (Frauenfelder and Steffen, 1965; Hemmingsen et al., 2004). The angular correlation between the two γ-rays depends on the properties of the nuclear decay while the perturbation - leading to the PAC acronym - is controlled by the interaction of the nucleus in the intermediate state (*i.e.* prior to the emission of the second γ-ray) with extra-nuclear magnetic fields or electric field gradients. Thus, in the absence of magnetic fields, measuring the perturbed angular correlation of the two γ-rays allows for the determination of the nuclear quadrupole interaction (NQI) of the PAC probe in the intermediate nuclear state.

The radioactive emission of metallic radionuclides can be exploited to image and treat cancer if they are firmly coordinated *via* a chelating agent to a biologically-active vector (*e.g.* peptide, antibody) capable to direct the location of the radionuclide mainly towards tumors, thus minimizing the damage of surrounding healthy sites (Price and Orvig, 2014; Ramogida and Orvig, 2013; Tosato et al., 2020a, 2021, 2022). A solid understanding of the stability of the radionuclide complexes *in vivo* is pivotal to obtain safe and effective radiopharmaceuticals. However, the conventional methods to attain information on the integrity of these radioactive complexes often rely on non-radioactive surrogates under conditions that do not always properly simulate the biological media. Since PAC is sensitive to the changes in the local environment of the nucleus, and because most biological material is relatively transparent to γ-rays, PAC spectroscopy can be a useful tool to non-invasively investigate the fate of a radionuclide attached to a carrier molecule under very low concentrations (10^{-12} M) and truly biologically relevant

* Corresponding author.
E-mail address: lhe@chem.ku.dk (L. Hemmingsen).

https://doi.org/10.1016/j.apradiso.2022.110508
Received 4 August 2022; Received in revised form 4 October 2022; Accepted 5 October 2022
Available online 13 October 2022

conditions.

Applications of PAC in the field of radiopharmaceuticals are rather limited and have mainly been conducted with compounds labeled with ^{111}In ($t_{1/2}$ = 2.83 days), a radioisotope also suitable for single photon emission computed tomography (SPECT) imaging (Kurakina et al., 2020; Marsden et al., 1991; Ramogida and Orvig, 2013; Smith et al., 1987). Unfortunately, ^{111}In often gives PAC spectra with low information content due to the so-called "after effects" derived from the ^{111}In to ^{111}Cd nuclear decay, that give rise to relaxation phenomena obscuring the PAC spectra (Hemmingsen et al., 2004 and references therein; Haas and Shirley, 1973) or can even trigger the degradation of the original molecular structure (Kurakina et al., 2020; Shpinkova et al., 2002).

^{111}Ag ($t_{1/2}$ = 7.45 days) is an unconventional radiometal that could be employed for cancer therapy and associated SPECT imaging (Aweda et al., 2013; Chattopadhyay et al., 2008; Tosato et al., 2020a). It may also be used in PAC spectroscopy, although only a limited number of ^{111}Ag-PAC publications exist to date (Balogh et al., 2020, 2022; Haas and Shirley, 1973; Hemmingsen et al., 2004 and references therein; Liu et al., 2008; Sas et al., 2006). This may be partially due to the fact that only a very small fraction of the ^{111}Ag-decays is "PAC active", *i.e.* pass through the γ-γ-cascade which is measured in the PAC experiment (*vide infra*), and thus a ^{111}Ag-PAC measurement typically requires at least several hours to achieve a decent signal-to-noise ratio. Moreover, from a radiopharmaceutical perspective, the lack of suitable Ag(I) chelators has reduced the interest toward this radionuclide so far, limiting its application in drug design and pre-clinical research. On the other hand, ^{111}Ag-PAC spectra are in general significantly less affected by deleterious "after effects" than ^{111}In-PAC spectra, and the ^{111}Ag half-life is long enough to carry out the potentially time-consuming radiochemical processes and to allow its delivery to more distant PAC-measurement facilities. As a result, ^{111}Ag may in some cases become an attractive alternative to ^{111}In.

In an attempt to address the challenge of stable ^{111}Ag(I) chelation, we have recently proposed a class of ligands established by a cyclen backbone with sulfur-containing pendant arms (Fig. 1) (Tosato et al., 2020a, 2020b). Among the investigated chelators, the most promising results were obtained with 1,4,7,10-tetrakis[2-(methylsulfanyl)ethyl]-1,4,7,10-tetraazacyclododecane (DO4S) (Tosato et al., 2020a). DO4S formed the most thermodynamically stable Ag(I) complexes, and it was able to quantitatively bind ^{111}Ag at 50°C and physiological pH (Tosato et al., 2020a).

This work aims to illustrate the potential of ^{111}Ag-PAC to provide insight on the structure and stability of ^{111}Ag-labeled compounds in biological environments. To accomplish this, we have simulated the ^{111}Ag-PAC signals for ^{111}Ag(I) bound to molecules having different molecular weights, and therefore displaying tumbling rates (rotational diffusion) on different time scales. The simulated spectra show how different scenarios may be elucidated, for example: ^{111}Ag(I) is stably coordinated by a low-molecular-weight probe represented by a single chelator moiety, or the ^{111}Ag-chelator complex is not stable *in vivo* and ^{111}Ag is transchelated by a high-molecular-weight protein. Next, these spectra were compared to the PAC experimental data obtained from a pilot study in which solutions of ^{111}Ag(I) bound DO4S and ^{111}Ag(I) in human serum, representative of each scenario, were analyzed. We hope this may serve as inspiration for future application of *in vivo* ^{111}Ag-PAC studies, including the design of chelators, and the evaluation of the stability of ^{111}Ag-labeled radiotracers.

2. Materials and methods

2.1. General

All solvents and reagents were purchased from commercial suppliers (Sigma-Aldrich, Fluka, VWR Chemicals) and were used without further purification. 1,4,7,10-Tetrakis[2-(methylsulfanyl)ethyl]-1,4,7,10-tetraazacyclododecane (DO4S) was synthesized in our laboratories according to previously reported procedures (Tosato et al., 2020b). Human serum was obtained after centrifugation from the blood of a healthy volunteer and stabilized by the addition of heparin. The human serum sample was kept in the refrigerator when not used.

2.2. Silver-111 production and purification

Silver-111 was produced by neutron irradiation of isotopically enriched palladium-110 (98.6% Pd-110, Oak Ridge National Lab, batch 214301) at the Institut Laue-Langevin (Grenoble, France) as previously described (Tosato et al., 2020a). Briefly, metallic palladium powder (3 mg) was enclosed in a quartz ampoule and irradiated for 7 days in a thermal neutron flux of 1.2 × 10^{15} $cm^{-2}s^{-1}$ in the beam tube V4 of the high flux reactor. Thermal neutron capture on ^{110}Pd produced ^{111}Pd ($t_{1/2}$ = 23.4 min) *via* the ^{110}Pd(n,γ)^{111}Pd reaction. The short-lived ^{111}Pd then decayed to ^{111}Ag.

The purification procedure was performed using an anion exchange column (Dowex 1x8) after the dissolution of the irradiated powder in *aqua regia* as reported in the literature (Bauer et al., 1997). ^{111}Ag(I) was selectively eluted by using 6 M HCl acid in several fractions containing different amounts of radioactivity. Fractions were concentrated by evaporation, and then added with a proper amount of water. ^{111}Ag(I) was provided as 1 M HCl samples.

2.3. Preparation of samples for ^{111}Ag-PAC spectroscopy

The samples for PAC spectroscopy were prepared as follows. An aqueous solution of $^{nat}AgNO_3$ (0.01 M) containing an aliquot of ^{111}Ag(I) in 1 M HCl (5–20 MBq) was added to a mixture containing (a) disodium phosphate solution (0.1 M), (b) disodium phosphate solution (0.1 M) and an aqueous solution of DO4S (10^{-3} M) in 1:1 metal-to-ligand molar ratio, (c) a disodium phosphate solution (0.1 M) and an aqueous solution of DO4S (10^{-3} M) in 2:1 metal-to-ligand molar ratio, and (d) diluted human serum. A detailed composition of each sample is reported in Table S1.

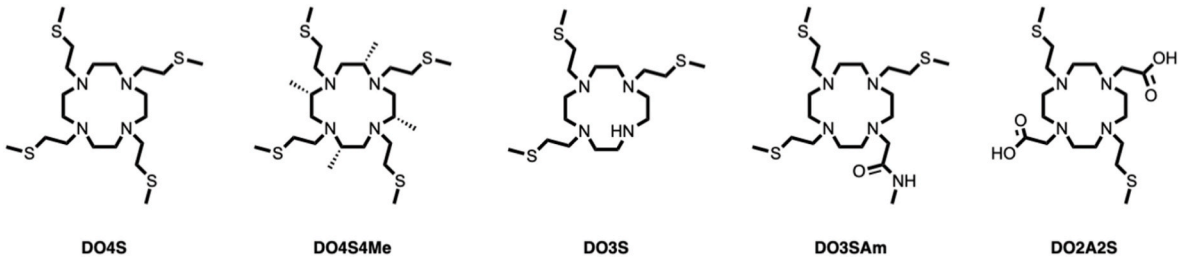

Fig. 1. Structure of the cyclen-based chelators with S-containing pendant arms: 1,4,7,10-tetrakis[2-(methylsulfanyl)ethyl]-1,4,7,10-tetraazacyclododecane (DO4S), (2S,5S,8S,11S)-2,5,8,11-tetramethyl-1,4,7,10-tetrakis[2-(methylsulfanyl)ethyl]-1,4,7,10-tetraazacyclododecane (DO4S4Me), 1,4,7-tris[2-(methylsulfanyl)ethyl]-1,4,7,10-tetraazacyclododecane (DO3S), 1,4,7-tris[2-(methylsulfanyl)ethyl]-10-acetamido-1,4,7,10-tetraazacyclododecane (DO3SAm), 1,7-bis[2-(methylsulfanyl)ethyl]-4,10,diacetic acid-1,4,7,10-tetraazacyclododecane (DO2A2S) (Tosato et al., 2020a, 2020b).

2.4. PAC instruments and data analysis

A digital PAC setup, DIGIPAC (Nagl et al., 2010), using five 1.5"×1.5" $LaBr_3$(Ce) detectors, was used for the spectroscopic measurements. The time resolution was 0.9 ns for the combined γ-γ coincidences, and the time-per-channel was 0.7910 ns. The initial data processing was conducted with the software PacMan and PacMaster (Nagl et al., 2010, 2011). All measurements were conducted with the samples at room temperature but otherwise kept in a refrigerator.

The data analysis and the simulation of PAC spectra were carried out with the Winfit program (provided by prof. T. Butz) using 550 data points (the first 10 points were always excluded due to systematic errors). A Lorentzian line shape was used with the parameter δ accounting for line broadening due to a static distribution of electric field gradients (EFGs).

All spectra were initially analyzed with two nuclear quadrupole interactions (NQIs), one with slow (or no) molecular reorientation and one with rapid molecular reorientation. Only NQIs with amplitude above the noise level (*i.e.* amplitude larger than the standard deviation) were kept in the final fit.

The experimental equivalent of $G_{22}(t)$ (*vide infra*) to which the NQI parameters are fitted is (1):

$$R(t) = 2\frac{W(180°,t) - W(90°,t)}{W(180°,t) + 2W(90°,t)} \quad (1)$$

where $W(180°,t)$ and $W(90°,t)$ are the geometrical mean of coincidence spectra recorded with 180° and 90° between detectors, after adjustment to the same ($t = 0$) start channel and correction for random coincidences.

2.5. ^{111}Ag-PAC theory

The decay scheme of ^{111}Ag is shown in Fig. 2. For the vast majority, ^{111}Ag directly decays to the ^{111}Cd ground state ($I = 1/2^+$) by β^--emission. However, 7% of the decays populate the ^{111}Cd excited state ($I = 3/2^+$, $E = 342$ keV) which subsequently has a 1.4% relative probability of decaying to the ground state by the emission of two consecutive γ-rays used in ^{111}Ag-PAC spectroscopy. Note that it is the nuclear quadrupole interaction (NQI) in the ^{111}Cd intermediate state ($I = 5/2^+$, $E = 245$ keV) which is probed in ^{111}Ag-PAC spectroscopy.

The β-decay of ^{111}Ag is accompanied by recoil energy of the ^{111}Cd daughter nucleus of up to around 500 kJ/mol, *i.e.* comparable to chemical bond energies. Moreover, the change of element and oxidation state from Ag(I) to Cd(II) in itself leaves the system out of equilibrium. Therefore, a significant amount of energy is deposited locally at the PAC probe site, and one cannot a priori exclude that the metal ion dissociates from the complex. However, ^{111}Ag PAC data on metal sites in proteins (Balogh et al., 2020; Hemmingsen et al., 2004) indicate that the ^{111}Cd (II) usually remains at the metal ion binding site, although the coordination geometry may change within a few hundreds of nanoseconds after the decay. Similarly, quantum chemical molecular dynamics simulations indicate that the kinetic energy is dissipated within picoseconds (Fromsejer et al., 2022), but that the local metal site structure may change to accommodate Cd(II). For static and randomly oriented molecules, the NQI is essentially characterized by two parameters, typically presented as the interaction strength (ω_0) and the asymmetry parameter (η).

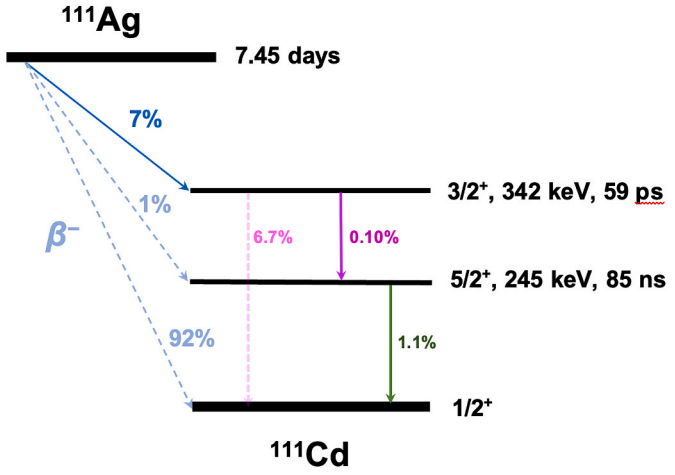

Fig. 2. Decay scheme for ^{111}Ag. Absolute β and γ-ray intensities are given in % per ^{111}Ag decay, additional intensity proceeds *via* emission of conversion electrons that are not detected in this work. In this work the 97–245 keV γ-γ cascade from the ^{111}Cd 342 keV excited state, which occurs in 0.1% of the ^{111}Ag decays, is used for PAC spectroscopy (Collins et al., 2014; 2016).

For each species, the parameter δ accounts for minor static structural variations from one molecule to the next, giving rise to the so-called static line broadening, and A^{eff} describes the effective amplitude of the signal, which is constant for a given radionuclide and given sample-detector geometry. Finally, λ reflects the characteristic rate of stochastic dynamics, such as molecular rotational diffusion. For a more thorough description of PAC parameters, we refer the reader to the literature (Hemmingsen et al., 2004).

The perturbation function for randomly oriented molecules and in the slow dynamics time regime ($\omega_0 \gg \lambda$) for a PAC isotope with spin $I = 5/2$ of the intermediate state is given by (2):

$$A^{eff}G_{22}(t) = A^{eff}e^{-\lambda t}(a_0 + a_1\cos(\omega_1 t) + a_2\cos(\omega_2 t) + a_3\cos(\omega_3 t)) \quad \omega_0 \gg \lambda \quad (2)$$

where a_i and ω_i depend on the quadrupole frequency (ω_0) and the asymmetry parameter (η) of the NQI. Thus, in this time regime, the perturbation function exhibits damped oscillations given by the three cosine functions and the exponential damping factor.

In the fast dynamics time regime ($\omega_0 \ll \lambda$) the perturbation function becomes a purely exponentially decaying function given by (3):

$$A^{eff}G_{22}(t) = A^{eff}e^{-2.8\frac{\omega_0^2}{\lambda}\left(1+\frac{\eta^2}{3}\right)t} \quad (3)$$

Note that the decay rate is determined by ω_0, η, and λ, but that these parameters cannot be determined independently in a single experiment. In the intermediate time regime ($\omega_0 \approx \lambda$) there is no analytical expression for the perturbation function, but it can be modelled numerically (Danielsen et al., 2002; Zacate and Hemmingsen, 2021).

2.6. Molecular rotational diffusion

In a simple model, the molecular dynamics may be described as exclusively originating from rotational diffusion with a characteristic rotational correlation time (τ_c) defined as (4):

$$\tau_c = \frac{1}{\lambda} \quad (4)$$

i.e. neglecting the intramolecular motion.

The rotational correlation time may be determined for spherical molecules using the Stokes-Einstein-Debye (SED) relation (5) (Perrin, 1934; Lavalette et al., 1999):

$$\tau_c^{SED} = \frac{V\xi}{kT} = \frac{4\pi(r_m + r_h)^3\xi}{3kT} \quad (5)$$

where V is the effective molecular volume of the molecule with radius r_m, typically including a hydration layer of radius r_h (which was set to $r_h = 3$ Å), ξ is the viscosity, k is Boltzmann's constant, and T is the absolute temperature. The molecular radius may be determined as (6):

$$r_m = \left(\frac{3M}{4\pi\rho N_A}\right)^{1/3} \quad (6)$$

where M is the molecular mass, ρ is the density of the molecule, and N_A is the Avogadro's number. The density depends on the investigated molecules and, in this study, it was set equal to the density of water at room temperature (1 g/cm^3). The choice of $\rho = 1$ g/cm^3 and $r_h = 3$ Å has no significant impact on the conclusions in this work.

For small molecules, the SED assumption of a homogenous distribution of mass throughout the rotating spherical molecule breaks down, and the mass displaying rotational diffusion may be smaller than the molecular mass. This situation includes for example a complex formed by a central heavy metal ion in water surrounded by 6 coordinating water molecules.

3. Results and discussion

3.1. Simulated ^{111}Ag-PAC spectra

The simulated ^{111}Ag-PAC data are presented in Fig. 3 for two sets of typical NQI parameters ($\omega_0 = 100$ Mrad/s and $\eta = 0$, panel A; $\omega_0 = 500$ Mrad/s and $\eta = 0$, panel B) for ^{111}Ag bound to molecules with molecular masses spanning from 100 g/mol to 1000000 g/mol in aqueous solution and at room temperature. As previously indicated, the perturbation function is exponentially decaying in the rapid rotational diffusion time regime (small molecules) and exhibits damped oscillations in the slow rotational diffusion time regime (large molecules). Consequently, the change of the PAC signal with the molecular mass demonstrates that PAC spectroscopy is sensitive to changes in rotational diffusion over 4 orders of magnitude of molecular mass of the molecule that binds ^{111}Ag.

For the low frequency series ($\omega_0 = 100$ Mrad/s, $\eta = 0$, Fig. 3 - panel A), the slow reorientation time regime is observed for molecular masses >100000 g/mol, while the signal is heavily damped in the range 10000-40000 g/mol. Finally, the rapid reorientation time regime is found for molecular masses <4000 g/mol. *In vitro*, these ranges can be shifted in a controlled manner by changing the temperature or viscosity of the solution. However, *in vivo* - for example in blood - the span of possible temperatures and viscosities are more limited, typically changing the rotational correlations time by no more than a factor of 10 from those indicated in Fig. 3. For instance, an increase of viscosity by a factor of 4 would roughly shift the ranges indicated above towards lower molecular masses by the same factor, *i.e.* slow rotational diffusion for molecular masses >25000 g/mol, intermediate for molecular masses = 1000–2500 g/mol, and fast rotational diffusion for molecular masses <1000 g/mol. The low frequency PAC signal is desirable in the sense, that changes in molecular mass as small as a factor of 2 (*i.e.* the labeled molecule binds to another molecule of the same molecular mass) give rise to significant changes in the PAC signal across almost the entire range of molecular masses. On the other hand, the high frequency PAC signal ($\omega_0 = 500$ Mrad/s, $\eta = 0$, Fig. 3 - panel B), remains in the information-rich, slow reorientation time regime for smaller molecular masses. However, once the molecular mass is < 10000 g/mol, the signal is strongly damped, and essentially remains damped for all the smaller molecular masses. This is an effect of the frequency, ω_0, entering the exponent quadratically (equation (3)), *i.e.* high frequency signals fall into a loss-of-signal "darkness" for molecular masses <10000 g/mol. This effect can in some cases be advantageous, for instance when a ^{111}Ag-labeled small molecule (giving practically no signal) binds to a large molecule such as a protein, thereby giving rise to the emergence of a signal, in analogy to a fluorescent probe lighting up upon binding.

In most bio-applications of PAC spectroscopy in the literature, sucrose is added to the solution to increase the viscosity, aiming to slow down the rotational diffusion and thereby ensuring that the system is in the slow dynamics time regime (Hemmingsen et al., 2004 and references therein). This is desirable because the damped oscillatory PAC signal (in the slow dynamics time regime) is more information-rich than the heavily damped signal (in the intermediate time regime) and the exponentially decaying signal (in the rapid dynamics time regime). Indeed, in the slow dynamics time regime, all three PAC parameters reflecting structure and dynamics (*i.e.* ω_0, η, and λ) can be determined independently. On the other hand, the significant change in the PAC signal with the change of molecular mass may be exploited to monitor the dynamics experienced by the PAC probe. As an example, this was reported for the binding of plastocyanin to photosystem 1, which is part of the electron transport in photosynthesis (Danielsen et al., 1999). In

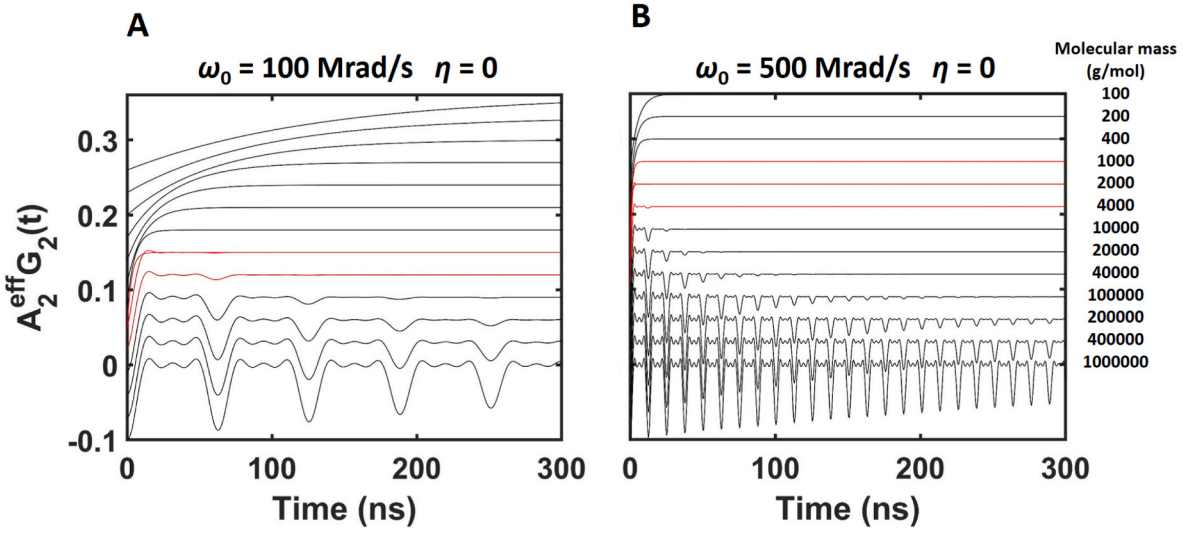

Fig. 3. Simulated ^{111}Ag-PAC perturbation functions for different molecular masses (indicated to the right) of the molecule to which ^{111}Ag is bound, and two different representative sets of ^{111}Ag-PAC parameters. Panel A: $\omega_0 = 100$ Mrad/s, $\eta = 0$. Panel B: $\omega_0 = 500$ Mrad/s, $\eta = 0$ ($A^{eff} = -0.1$ in both panels, and the plots of the individual perturbation functions are shifted vertically by 0.03 units each to facilitate visual inspection). τ_c is calculated according to the Stokes-Einstein-Debye approximation (see Table S2) using $r_h = 3$ Å, $\rho = 1$ g/cm^3, $\xi = 1.0$ mPa s, $T = 298.15$ K, and the molecules are assumed to be rigid (*i.e.* no intramolecular dynamics). Perturbation functions above the red lines are calculated within the fast molecular reorientation approximation (low molecular masses) and exhibit pure exponential decay. Perturbation functions below the red lines are calculated within the slow molecular reorientation approximation (high molecular masses) and exhibit damped oscillations. Perturbation functions indicated in red are in the intermediate time regime, where neither of the two approximations are valid. Notice that the dynamic range in which the PAC signal is sensitive to molecular mass spans several orders of magnitude. (For interpretation of the references to colour in this figure legend, the reader is referred to the Web version of this article.)

aqueous solution ^{111}Ag(I) bound to plastocyanin (molecular mass ~ 10000 g/mol) gives a strongly damped PAC signal (intermediate time regime), as expected from Fig. 3. However, upon the addition of the large photosystem 1 to the sample, the rotational diffusion was significantly slowed down, and a damped oscillatory signal was observed, thereby demonstrating the formation of the plastocyanin-photosystem 1 complex.

At the other extreme, it is possible to change from the rapid dynamics time regime to the intermediate time regime. In the limit of very rapid rotational diffusion or very low frequency NQIs, the exponent $(-2.8\omega_0^2(1+\eta^2/3)/(\lambda t))$ of equation (3) converges to 0, thereby leaving the angular correlation unperturbed (*i.e.* $G_{22}(t) = 1$), in contrast to the rapid loss of signal occurring in the intermediate dynamics time regime where $G_{22}(t)$ approaches to 0 within the first short time span, *i.e.* within about the first 10 ns of $G_{22}(t)$. This situation was exploited to study the binding of Cd(II) to the enzyme superoxide dismutase (SOD) (Bauer et al., 1991). The Cd(II)-SOD complex displayed dynamics in the intermediate time regime (*i.e.* a strongly damped perturbation function) while free Cd(II) in solution essentially gave $G_{22}(t) = 1$ presumably reflecting both a low frequency NQI (assuming that the aqua ion of Cd (II) coordinates six water molecules in an octahedral coordination geometry) and rapid rotational diffusion, thereby allowing for discrimination of free Cd(II) in solution and Cd(II) bound to SOD. In that study, the authors used the so-called time integrated PAC spectroscopy (TI-PAC) recording the integral of the PAC signal over the first 150 ns of the perturbation function. The main advantage of TI-PAC is that a decent S/N may be achieved considerably faster than when recording the full-time dependence of the perturbation function. In many cases, TI-PAC may also be the method of choice for ^{111}Ag-PAC spectroscopy, in particular, because of the long time necessary (hours to days) to record a time-dependent PAC spectrum for this isotope.

3.2. Experimental ^{111}Ag-PAC spectra

In this section we present a pilot ^{111}Ag-PAC study with examples of spectra, which as it turned out, fall into the three-time regimes of rotational reorientation presented above (*i.e.* slow, intermediate, and fast), thus illustrating the span of spectroscopic features that may be encountered *in vivo*.

^{111}Ag-PAC spectra were recorded for solutions containing: (a) [^{111}Ag]Ag(I) in buffered solution, (b, c) [^{111}Ag]Ag(I) in presence of DO4S in two different metal-to-ligand molar ratios, and (d) [^{111}Ag]Ag(I) in human serum. The resulting spectra are shown in Fig. 4 from which the parameters in Table 1 are determined. Although, the S/N obtained in this pilot study is not impressive, it is adequate for the conclusions presented in the following sections. The S/N may be improved by increasing the ^{111}Ag activity in the samples. In this work the ^{111}Ag activity of each sample was on the order of 1 MBq by the start of the PAC measurement, which typically lasted a 1–5 days. The activity can be increased by at least an order of magnitude without saturating the detectors and introducing excessive dead-time. The amount of ^{111}Ag produced by neutron irradiation of isotopically enriched ^{110}Pd is not a limitation, as typical batch activities by the end of production are on the order of 1 GBq and can be further increased if required. Thus, it is feasible to achieve better S/N than obtained for in the samples in the present work.

The ^{111}Ag-PAC signal of [^{111}Ag]Ag(I) added to the phosphate buffered solution with no chelator present (Fig. 4 - red line and Table 1 - sample a) exhibits damped oscillatory behavior and can be analyzed with one static NQI. The data, therefore, indicate that Ag(I) is precipitated or embedded in very large complexes. The low frequency and high asymmetry of the NQI ($\omega_0 = 142(5)$ Mrad/s, $\eta = 0.73(7)$) indicate that Ag(I) occupies a site with coordination number >2, akin to low frequency signals observed for non-linear coordination, *e.g.* observed in $AgNO_3(s)$ and $Ag_2SO_4(s)$ (Lerf and Butz, 1987). The damping of the PAC signal can either be due to a number of different inequivalent Ag(I) sites

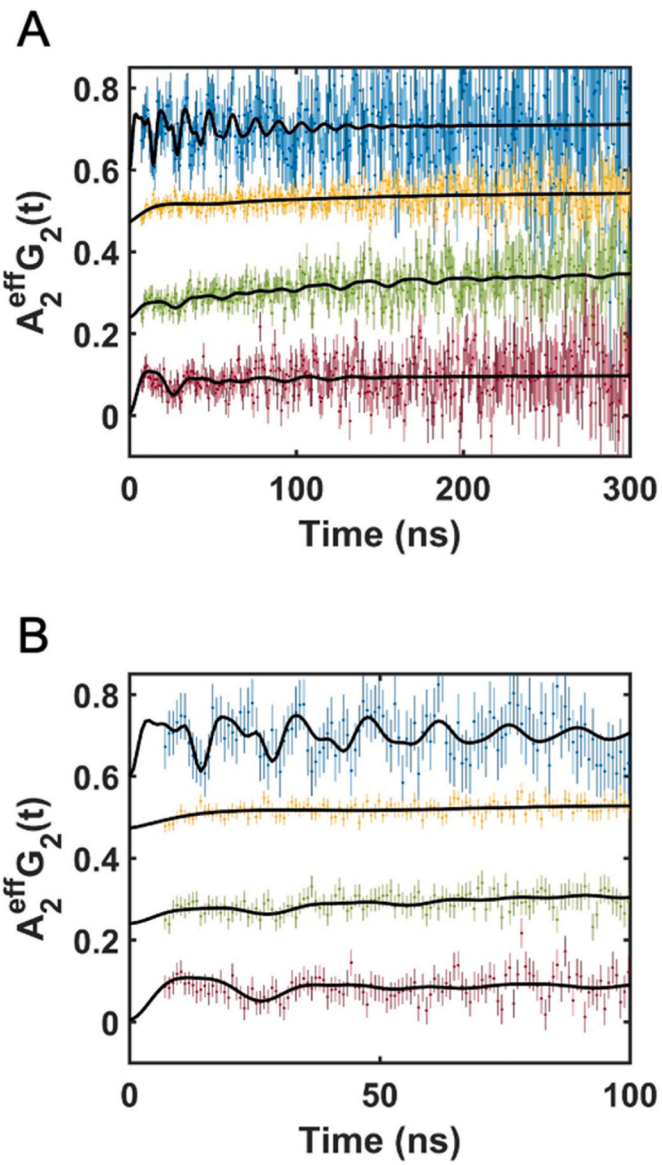

Fig. 4. ^{111}Ag-PAC data and fit (bold faced line). (A) Time scale from 0 to 300 ns; (B): Zoom-in on the first 100 ns (included for a better visual evaluation of the initial oscillatory signals). Red: [^{111}Ag]Ag(I) in buffered solution (sample a); green: [^{111}Ag]Ag(I) in presence of DO4S in a 1:1 metal-to-ligand ratio (sample b); yellow: [^{111}Ag]Ag(I) in presence of DO4S in 1:0.5 metal-to-ligand ratio (sample c); blue: [^{111}Ag]Ag(I) in human serum (sample d). (For interpretation of the references to colour in this figure legend, the reader is referred to the Web version of this article.)

Table 1
Parameters fitted to ^{111}Ag-PAC data (see main text and Fig. 4). Sample conditions are described in detail in the methods section.

Sample	ω_0 (Mrad/s)	η	δ × 100	λ μs^{-1}	c^a μs^{-1}	A × 100	χ_r^2
(d)	435(7)	0.22(5)	3(1)	2(6)	NA	−13(4)	0.57
(c)	NA	NA	NA	NA	9(3)	−4.1(5)	0.72
(b)	133(2)	0.78(4)	0(5)	4(14)	NA	−2(1)	0.64
	NA	NA	NA	NA	9(2)	−9(1)	
(a)	142(5)	0.73(7)	5(6)	11(11)	NA	−9(3)	0.71

[a] c is the decay rate of the exponentially decaying signal appearing in the fast dynamics time regime, see eq. (3), $c = 2.8\frac{\omega_0^2}{\lambda}\left(1+\frac{\eta^2}{3}\right)$.

in the precipitate, rotational diffusion (for nanosized particles), or to the recoil experienced by the ^{111}Cd daughter nucleus after the β^- decay, causing Cd(II) to occupy various binding sites with different local structure.

The main component of the PAC signal of [^{111}Ag]Ag(I) in presence of DO4S in a 1:1 M ratio (Fig. 4 - green line and Table 1 - sample b), is an exponentially decaying signal, accounting for ~ 80% of the total signal. This signal falls in the fast dynamics time regime illustrated in the upper part of Fig. 3 - panel A (*i.e.* in the opposite extreme as compared to Ag(I) in human serum - *vide infra*). This signal is in accordance with Ag(I) bound to the rapidly tumbling chelator, and indicates that the majority of Ag(I) is in the form of $[Ag(DO4S)]^+$ (and not precipitated) under these conditions, as expected (Tosato et al., 2020a). The exponentially decaying signal which presumably originates from Ag(I)-DO4S is significantly different from the signal recorded for Ag(I) with no chelator present, hence, at the phenomenological level, precipitated Ag(I) in buffered solution can be discriminated from Ag(I) bound to a chelator in solution. Only the decay constant, $c = 2.8(\omega_0)^2/(\lambda)(1+\eta^2/3)$ can be extracted from the data in this case of fast dynamics, giving $c = 9$ (2) μs^{-1}. If the effective rotating molecular mass of the Ag(I)-chelator complex and the hydration layer are assumed to be 600 g/mol and 3 Å, respectively, the calculated rotational correlation time (τ_c) is 0.8 ns. This result gives an estimated $\omega_0 = 60$ Mrad/s (assuming that $\eta = 0$) which is in qualitative agreement with ω_0 expected for the previously reported structure of $[Ag(DO4S)]^+$, *i.e.* a complex in which Ag(I) is six coordinated with four ammines and two exchanging thioethers (Gyr et al., 1997; Tosato et al., 2020a). There is another low amplitude component accounting for the remaining ~ 20% of the signal, which is very similar to the one recorded for sample (a), indicating that a minor fraction of Ag(I) is not bound to DO4S and remains in the structure observed for Ag(I) in sample (a).

The main component of the PAC signal of the [^{111}Ag]Ag(I) solution in presence of DO4S in a 1:0.5 M ratio (Fig. 4 - yellow line and Table 1 - sample c), gives a signal with the same characteristic exponential decay as sample (b), presumably again reflecting the presence of the $[Ag(DO4S)]^+$ complex (*vide supra*). However, the amplitude of this signal, $A = -0.041(5)$, is significantly lower than the amplitude of the same signal in sample (b), where the total amplitude is $-0.11(2)$ ($= -0{,}02 - 0{,}09$, Table 1). In PAC spectroscopy the total amplitude of the signal for a given radionuclide and at a fixed sample-detector geometry is constant. Thus, there is a missing fraction of the signal for sample (c), *i.e.* about half of the signal which is not accounted for. This strongly indicates that the remaining part of the signal decays to zero within the first 5–10 ns, *i.e.* a situation illustrated with the red lines in Fig. 3, representing dynamics on the intermediate time scale. This finding is in agreement with the experimental conditions of 1:0.5 metal:chelator molar ratio, *i.e.* that half of the Ag(I) is bound to the chelator, while the rest is free in solution. Note that the pH for this sample was around 5.0, and this lower pH presumably shifts the equilibrium of the precipitate observed in sample (a) (pH = 6.7) towards species in solution, which then display rotational diffusion on the intermediate time scale, giving rise to the missing fraction of the PAC signal. This demonstrates that PAC spectroscopy may provide quantitative results on the radiochemical incorporation efficiency, complementing the more commonly used radio-thin layer chromatography (TLC) or radio-high performance liquid chromatography (HPLC) analyses.

The ^{111}Ag-PAC signal for [^{111}Ag]Ag(I) in human serum (Fig. 4 - blue line and Table 1 - sample d), displays a high frequency NQI and slow rotational diffusion, indicating that Ag(I) is either bound to large biomolecules or precipitated, but not bound to low molecular mass species. Thus, this signal falls in the range illustrated in the lower part of Fig. 3 - panel B.

The high frequency ($\omega_0 = 435(7)$ Mrad/s) and low asymmetry parameter ($\eta = 0.2(1)$), is similar to the ^{111}Ag-PAC signal reported for a single crystal of $[Ag(imidazole)_2]NO_3(s)$ ($\omega_0 = 425.5(1)$ Mrad/s, $\eta = 0.240(1)$ (Hansen et al., 1999)), where Ag(I) occupies an almost linear coordination geometry with two coordinating imidazoles. This finding is in a good agreement with a bis-histidine linear coordination proposed for Cu(I) when binding to human serum albumin (HSA) (Sendzik et al., 2017). Thus, in analogy to Cu(I), it is conceivable that Ag(I) is bound to the same albumin binding site. Moreover, HSA constitutes the main carrier protein of human serum at a concentration of ~ 0.6 mM (the concentration of Ag(I) in our experiment was 47 μM) and it is plausible that it transports Ag(I) ions as it does with other metals. On the other hand, the fitted inverse rotational correlation time, λ_{slow} ($= 1/\tau_c$) $= 2(6)$ μs^{-1}, is rather low, assuming that Ag(I) is bound to HSA (molecular mass of 66500 g/mol) and would correspond to an Ag(I) binding species with an estimated molecular mass of ~ 610000 g/mol (using a viscosity of 1.8 mPa s at RT for human serum). The S/N of the current data and the large error bar on λ_{slow} do not allow for reliable conclusions on this matter although it is possible that Ag(I) induces aggregation of HSA (Alhazmi et al., 2021) or that the long time needed for the PAC measurement caused clustering of the plasmatic proteins. An alternative interpretation could be, that Ag(I) is precipitated in the form of Ag_2O and, although no ^{111}Ag-PAC data have been reported for this compound, the linear Ag(I) two-coordination in Ag_2O is likely to give a high frequency PAC signal similar to the observed NQI.

4. Conclusion

With this work we present simulated PAC spectra, illustrating the information that may be derived from ^{111}Ag-PAC experiments. We particularly focus on the effect of rotational diffusion on PAC spectra, and how changes in rotational correlation time (caused by changes in molecular mass of the ^{111}Ag binding species) may be observed. The qualitative appearance of the PAC spectra differs depending on the NQI and the characteristic rate of dynamics, λ, and is typically divided into the slow ($\omega_0 \gg \lambda$), intermediate ($\omega_0 \approx \lambda$), and fast ($\omega_0 \ll \lambda$) dynamics time regimes. A pilot series of ^{111}Ag PAC experiments were compared to the simulated spectra, and as it turns out, the experimental data include examples of both slow, intermediate, and fast dynamics. As such, the data illustrate that the PAC signal for ^{111}Ag(I) in human serum is significantly different from that for ^{111}Ag(I) bound to a small molecule like an Ag(I)-chelator. Therefore, ^{111}Ag-PAC spectroscopy may be applied to monitor the *in vivo* fate of a^{111}Ag-labeled compound.

In a broader perspective one may envisage: 1) stability studies of ^{111}Ag-radiopharmaceuticals, where the characteristic PAC signal, reflecting rapid molecular rotational diffusion, would indicate that ^{111}Ag(I) remains bound to the chelator, 2) dissociation studies of ^{111}Ag from the original compound followed by binding to another (bio) molecule of different molecular mass such as serum proteins, 3) binding studies of ^{111}Ag-based radiopharmaceuticals, where binding of a ^{111}Ag-labeled (small) molecule to another (large) molecule gives rise to a significant change in molecular mass and thereby in the rotational correlation time, 4) monitoring the *in vivo* lifetime of a molecular vehicle transporting ^{111}Ag-labeled radiotracer, such as lipid nanoparticles used to deliver drugs (Derksen et al., 1988; Forssen, 1997; Hwang and Mauk, 1977; Kamkaew et al., 2019; Mauk et al., 1980; Meares and Westmoreland, 1971; Roerdink et al., 1989), because ^{111}Ag will bind to (bio) molecules once the drug delivery agent degrades. A secondary point is that PAC spectroscopy may give insights into the metal coordination environment of the protein binding site, thus facilitating the identification of the carrier protein *in vivo*. Finally, PAC spectroscopy may be applied to analyze the binding of a radionuclide to a chelator, providing an alternative approach to the more common chromatographic methods.

CRediT authorship contribution statement

Marianna Tosato: Writing – review & editing, Investigation, Conceptualization. **Mattia Asti:** Writing – review & editing, Supervision, Methodology, Funding acquisition, Conceptualization. **Valerio Di**

Marco: Writing – review & editing, Supervision. **Marianne L. Jensen:** Investigation, Formal analysis. **Juliana Schell:** Investigation, Funding acquisition, Formal analysis, Data curation. **Thien Thanh Dang:** Investigation, Formal analysis. **Ulli Köster:** Supervision, Data curation, Investigation, Methodology, Resources, Writing - review & editing. **Mikael Jensen:** Resources, Investigation, Conceptualization. **Lars Hemmingsen:** Writing – original draft, Validation, Supervision, Resources, Project administration, Methodology, Investigation, Funding acquisition, Formal analysis, Data curation, Conceptualization.

Declaration of competing interest

The authors declare that they have no known competing financial interests or personal relationships that could have appeared to influence the work reported in this paper.

Data availability

Data will be made available on request.

Acknowledgements

The research leading to these results has received funding from the Danish Ministry of Higher Education and Science (NICE grant, grant number 7129-00001B) and was also funded by the German Federal Ministry of Education and Research (BMBF) through Contract No. 05K16PGA, by the Italian Ministry of Health as part of the program "5perMille, year 2020" promoted by the AUSL-IRCCS of Reggio Emilia (Italy) and by the Legnaro National Laboratories of the Italian Institute of Nuclear Physics ("ISOLPHARM_EIRA Project").

Appendix A. Supplementary data

Supplementary data related to this article can be found at https://doi.org/10.1016/j.apradiso.2022.110508.

References

Alhazmi, H.A., Ahsan, W., Ibrahim, A.M.M., Khubrani, R.A.Y., Haddadi, Z.A.A., Safhi, A. Y.F., Shubayr, N., Al Bratty, M., Najmi, A., 2021. Investigation of bovine serum albumin aggregation upon exposure to silver(I) and copper(II) metal ions using zetasizer. Open Chemistry 19, 987–997.

Aweda, T.A., Ikotun, O., Mastren, T., Cannon, C.L., Wright, B., Youngs, W.J., Cutler, C., Guthrie, J., Lapi, S., 2013. The use of ^{111}Ag as a tool for studying biological distribution of silver-based antimicrobials. Medchemcomm 4, 1015–1017.

Balogh, R.K., Gyurcsik, B., Jensen, M., Thulstrup, P.W., Köster, U., Christensen, N.J., Mørch, F.J., Jensen, M.L., Jancsó, A., Hemmingsen, L., 2020. Flexibility of the CueR metal site probed by instantaneous change of element and oxidation state from Ag(I) to Cd(II). Chem. Eur J. 26, 7451–7457.

Balogh, R.K., Gyurcsik, B., Jensen, M., Thulstrup, P.W., Köster, U., Christensen, N.J., Jensen, M.L., Hunyadi-Gulyás, E., Hemmingsen, L., Jancsó, A., 2022. Tying up a loose end: on the role of the C-terminal CCHHRAG fragment of the metalloregulator CueR. Chembiochem, e202200290.

Bauer, R., Bjerrum, M., Danielsen, E., Kofod, P., 1991. Coordination geometry of cadmium at the zinc and copper sites of superoxide dismutases: a study using perturbed angular correlation of gamma-rays from excited ^{111}Cd. Acta Chem. Scand. 45, 593–603.

Bauer, R., Danielsen, E., Hemmingsen, L., Bjerrum, M.J., Hansson, Ö., Singh, K., 1997. Interplay between oxidation state and coordination geometry of metal ions in azurin. J. Am. Chem. Soc. 119, 157–162.

Chattopadhyay, S., Vimalnath, K.V., Saha, S., Korde, A., Sarma, H.D., Pal, S., Das, M.K., 2008. Preparation and evaluation of a new radiopharmaceutical for radio synovectomy, Ag-111-Labelled hydroxyapatite (HA) particles. Appl. Radiat. Isot. 66, 334–339.

Collins, S., Keightley, J., Gilligan, C., Gasparro, J., Pearce, A., 2014. Determination of the gamma emission intensities of ^{111}Ag. Appl. Radiat. Isot. 87, 107–111.

Collins, S., Harms, A.V., Regan, P.H., 2016. Half-life determination of the ground state decay of 111Ag. Appl. Radiat. Isot. 108, 143–147.

Danielsen, E., Jørgensen, L.E., Sestoft, P., 2002. Monte Carlo simulations of PAC-spectra as a general approach to dynamic interactions. Hyperfine Interact. 141, 607–626.

Danielsen, E., Scheller, H.V., Bauer, R., Hemmingsen, L., Bjerrum, M.J., Hansson, Ö., 1999. Plastocyanin binding to photosystem I as a function of the charge state of the metal ion: effect of metal site conformation. Biochemistry 38, 11531–11540.

Derksen, J.T., Baldeschwieler, J.D., Scherphof, G.L., 1988. In vivo stability of ester- and ether-linked phospholipid-containing liposomes as measured by perturbed angular correlation spectroscopy. Proc. Natl. Acad. Sci. U.S.A. 85, 9768–9772.

Forssen, E.A., 1997. The design and development of DaunoXome® for solid tumor targeting in vivo. Adv. Drug Deliv. Rev. 24, 133–150.

Frauenfelder, H., Steffen, R.M., 1965. Alpha-, Beta- and Gamma-Ray Spectroscopy. North Holland, Amsterdam, p. 997.

Fromsejer, R., Haas, H., Mikkelsen, K.V., Hemmingsen, L., 2022. Calculations of electric field gradients in the gas phase for CdI_2 using BOMD simulations. Chem. Phys. Lett. 801, 139704.

Gyr, T., Mäcke, H.R., Hennig, M., 1997. A highly stable silver(I) complex of a macrocycle derived from tetraazatetrathiacyclen. Angew. Chem. 36, 2786–2788.

Haas, H., Shirley, D.A., 1973. Nuclear quadrupole interaction studies by perturbed angular correlations. J. Chem. Phys. 58, 3339–3355.

Hansen, B., Bukrinsky, J.T., Hemmingsen, L., Bjerrum, M.J., Singh, K., Bauer, R., 1999. Effects of the nuclear transformation ^{111}Ag(I) to ^{111}Cd(II) in a single crystal of Ag [^{111}Ag] (imidazole)$_2NO_3$. Phys. Rev. B 59, 14182–14190.

Hemmingsen, L., Sas, K.N., Danielsen, E., 2004. Biological applications of perturbed angular correlations of γ-ray spectroscopy. Chem. Rev. 104, 4027–4062.

Hwang, K., Mauk, M., 1977. Fate of lipid vesicles in vivo: a gamma-ray perturbed angular correlation study. Proc. Natl. Acad. Sci. U.S.A. 74, 4991–4995.

Kamkaew, A., Ehlerding, E.B., Cai, W., 2019. Nanoparticles as radiopharmaceutical vectors. In: Radiopharmaceutical Chemistry, pp. 181–203.

Kurakina, E.S., Radchenko, V., Belozub, A.N., Bonchev, G., Bozhikov, G.A., Velichkov, A. I., Stachura, M., Karaivanov, D.V., Magomedbekov, E.P., Filosofov, D.V., 2020. Perturbed angular correlation as a tool to study precursors for radiopharmaceuticals. Inorg. Chem. 59, 12209–12217.

Lavalette, D., Tétreau, C., Tourbez, M., Blouquit, Y., 1999. Microscopic viscosity and rotational diffusion of proteins in a macromolecular environment. Biophys. J. 76, 2744–2751.

Lerf, A., Butz, T., 1987. Nuclear quadrupole interactions in compounds studied by time differential perturbed angular correlations/distributions. Hyperfine Interact. 36, 275–370.

Liu, T., Chen, X., Ma, Z., Shokes, J., Hemmingsen, L., Scott, R.A., Giedroc, D.P., 2008. A Cu(I)-Sensing ArsR family metal sensor protein with a relaxed metal selectivity profile. Biochemistry 47, 10564–10575.

Marsden, P.J., Smith, F.A., Mather, S., 1991. A PAC study of the binding of ^{111}In to a monoclonal antibody via the macrocyclic molecule 1,4,7-triazacyclononanetriacetic acid. Int. J. Rad. Appl. Instrum. Part A. Appl. Rad. Isotop. 42, 815–822.

Maurk, M.R., Gamble, R.C., 1979. Stability of lipid vesicles in tissues of the mouse: a gamma-ray perturbed angular correlation study. Proc. Natl. Acad. Sci. U.S.A. 76, 765–769.

Mauk, M.R., Gamble, R.C., Baldeschwieler, J.D., 1980. Vesicle targeting: timed release and specificity for leukocytes in mice by subcutaneous injection. Science 207, 309–311.

Meares, C.F., Westmoreland, D.G., 1971. The study of biological macromolecules using perturbed angular correlations of gamma radiation. Cold Spring Harbor Symp. Quant. Biol. 36, 511–516.

Nagl, M., 2011. PAC-suite. http://pac-suite.sourceforge.net/pacsuite/html/index.html.

Nagl, M., Vetter, U., Uhrmacher, M., Hofsäss, H., 2010. A new all-digital time differential γ-γ angular correlation spectrometer. Rev. Sci. Instrum. 81, 073501.

Perrin, F., 1934. Brownian motion of an ellipsoid - I. Dielectric dispersion for ellipsoidal molecules. J. Phys. Radium 5, 497–511.

Price, E.W., Orvig, C., 2014. Matching chelators to radiometals for radiopharmaceuticals. Chem. Soc. Rev. 43, 260–290.

Ramogida, C.F., Orvig, C., 2013. Tumour targeting with radiometals for diagnosis and therapy. Chem. Commun. 49, 4720–4739.

Roerdink, F.H., Regts, J., Handel, T., Sullivan, S.M., Baldeschwieler, J.D., Scherphof, G. L., 1989. Effect of cholesterol on the uptake and intracellular degradation of liposomes by liver and spleen; A combined biochemical and γ-ray perturbed angular correlation study. Biochim. Biophys. Acta 980, 234–240.

Sas, K.N., Haldrup, A., Hemmingsen, L., Danielsen, E., Øgendal, L.H., 2006. pH-dependent structural change of reduced spinach plastocyanin studied by perturbed angular correlation of γ-rays and dynamic light scattering. J. Biol. Inorg. Chem. 11, 409–418.

Sendzik, M., Pushie, M.J., Stefaniak, E., Haas, K.L., 2017. Structure and affinity of Cu(I) bound to human serum albumin. Inorg. Chem. 56, 15057–15065.

Shpinkova, L.G., Carbonari, A.W., Nikitin, S.M., Mestnik-Filho, J., 2002. Influence of electron capture after-effects on the stability of ^{111}In(^{111}Cd)-Complexes with organic ligands. Chem. Phys. 279, 255–263.

Smith, F.A., Marsden, P.J., Mather, S., 1987. Indium binding to monoclonal antibodies: a study of Bifunctional chelates using perturbed angular correlations. Nucl. Instrum. Methods Phys. Res., Sect. A 255, 287–289.

Tosato, M., Asti, M., Dalla Tiezza, M., Orian, L., Häussinger, D., Vogel, R., Köster, U., Jensen, M., Andrighetto, A., Pastore, P., Di Marco, V., 2020a. Highly stable silver(I) complexes with cyclen-based ligands bearing sulfide arms: a step toward silver-111 labeled radiopharmaceuticals. Inorg. Chem. 59, 10907–10919.

Tosato, M., Dalla Tiezza, M., May, N.V., Isse, A.A., Nardella, S., Orian, L., Verona, M., Vaccarin, C., Alker, A., Mäcke, H., Pastore, P., Di Marco, V., 2021. Copper coordination chemistry of sulfur pendant cyclen derivatives: an attempt to hinder the reductive-induced demetallation in $^{64/67}$Cu radiopharmaceuticals. Inorg. Chem. 60, 11530–11547.

Tosato, M., Pelosato, M., Franchi, S., Isse, A.A., May, N.V., Zanoni, G., Mancin, F., Pastore, P., Badocco, D., Asti, M., Di Marco, V., 2022. When ring makes the difference: coordination properties of Cu^{2+}/Cu^{+} complexes with sulfur-pendant

polyazamacrocycles for radiopharmaceutical applications. New J. Chem. 46, 10012–10025.
Tosato, M., Verona, M., Doro, R., Dalla Tiezza, M., Orian, L., Andrighetto, A., Pastore, P., Marzaro, G., Di Marco, V., 2020b. Toward novel sulphur-containing derivatives of tetraazacyclododecane: synthesis, acid-base properties, spectroscopic characterization, DFT calculations, and cadmium(II) complex formation in aqueous solution. New J. Chem. 44, 8337–8350.
Zacate, M.O., Hemmingsen, L., 2021. Perturbed angular correlation spectra due to rotating electric field gradients. Hyperfine Interact. 242, 56.